analytical chemistry

pubs.acs.org/ac

Article

Light Extinction by Agglomerates of Gold Nanoparticles: A Plasmon Ruler for Sub-10 nm Interparticle Distances

Georgios A. Kelesidis, Daniel Gao, Fabian H.L. Starsich, and Sotiris E. Pratsinis*

Cite This: *Anal. Chem.* 2022, 94, 5310−5316

Read Online

ACCESS | Metrics & More | Article Recommendations

ABSTRACT: Plasmon rulers relate the shift of resonance wavelength, λ_l, of gold agglomerates to the average distance, s, between their constituent nanoparticles. These rulers are essential for monitoring the dynamics of biomolecules (*e.g.*, proteins and DNA) by determining their small (<10 nm) coating thickness. However, existing rulers for dimers and chains estimate coating thicknesses smaller than 10 nm with rather large errors (more than 200%). Here, the light extinction of dimers, 7- and 15-mers of gold nanoparticles with diameter d_p = 20−80 nm and s = 1−50 nm is simulated. Such agglomerates shift λ_l up to 680 nm due to plasmonic coupling, in excellent agreement with experimental data by microscopy, dynamic light scattering, analytical centrifugation, and UV−visible spectroscopy. Subsequently, a new plasmon ruler is derived for gold nanoagglomerates that enables the accurate determination of sub-10 nm coating thicknesses, in excellent agreement also with tedious microscopy measurements.

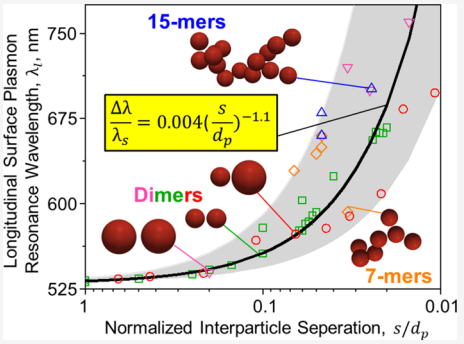

INTRODUCTION

Clusters (agglomerates) of Au nanoparticles (NPs) attract scientific attention for their unique optical properties that have a strong wavelength dependence due to oscillating surface electrons (*i.e.*, plasmons). Such clusters exhibit a longitudinal surface plasmon resonance at a wavelength λ_l due to plasmonic coupling[1] in addition to their transversal light extinction maximum,[2] λ_s, at 530 nm. The Au λ_l shifts to longer wavelengths as the interparticle distance, s, between two Au NPs (dimers) is reduced down to 1 nm[3]. This shift is achieved by coating the NPs with nanothin organic[4] or inorganic[5] films. Reducing s below 1 nm does not affect λ_l due to quantum tunneling[6] and a quenched near-field intensity.[7]

Plasmon rulers[3] describe the dependence of Au λ_l on s. They are used to select the film thickness onto these particles that are extracted using tedious microscopy[8] or unstable Förster resonance energy transfer measurements.[9] Such rulers enable monitoring of the conformational dynamics of bovine serum albumin,[10] fibrinogen, γ-globulin, histone, insulin,[11] mouse matrix metalloproteinase,[12] the heat shock protein 90,[13] and single[14] and double[15] stranded DNA molecules. A plasmon ruler has been used also to detect DNA molecules using surface-enhanced Raman spectroscopy.[16] Furthermore, plasmon rulers are essential for the optimization of the Au agglomerate efficiency in the photothermal treatment of cancers.[5]

Empirical plasmon rulers have been derived based on UV−visible spectroscopy of single[17] or dimer[10] Au NPs deposited on flat surfaces. Such relations facilitate the detection of organic coatings or films as thin as 0.4 nm[18] but have been used only for *in vitro* biomedical applications. This can be partly attributed to the wet chemistry methods used for the Au dimer synthesis that have not been scaled up yet[19] and limit their translation to clinical applications.[20] To this end, a plasmon ruler was obtained by discrete dipole approximation (DDA) simulations[3] of Au dimers with s > 10 nm. This ruler was used to accurately estimate thicknesses of DNA coatings[15] larger than 10 nm. However, at small s (<10 nm), the Au λ_l redshift[3] ($\Delta\lambda = \lambda_l - \lambda_s$) of 90 nm is up to 40% smaller than that measured[17] from Au dimers. In addition, the use of this ruler[3] for *in vivo* detection of organics is not trivial, as dimers further coagulate into larger agglomerates during their administration into the blood stream[21] and their internalization by cells.[22]

The morphology of such agglomerates is typically quantified by the fractal dimension, D_f, that rapidly attains its asymptotic 1.8 by coagulation within 100 ms[23] for the typical Au suspension concentrations employed in drug delivery.[21] During *in vivo* administration of gold NPs, hydrodynamic (*e.g.*, shear[24]), van der Waals, or electric forces[25] could break and reassemble these agglomerates,[21] increasing their D_f up to about 2 (Figure 8 in ref 24). The extinction spectra of such

Received: November 27, 2021
Accepted: March 11, 2022
Published: March 21, 2022

https://doi.org/10.1021/acs.analchem.1c05145
Anal. Chem. 2022, 94, 5310−5316

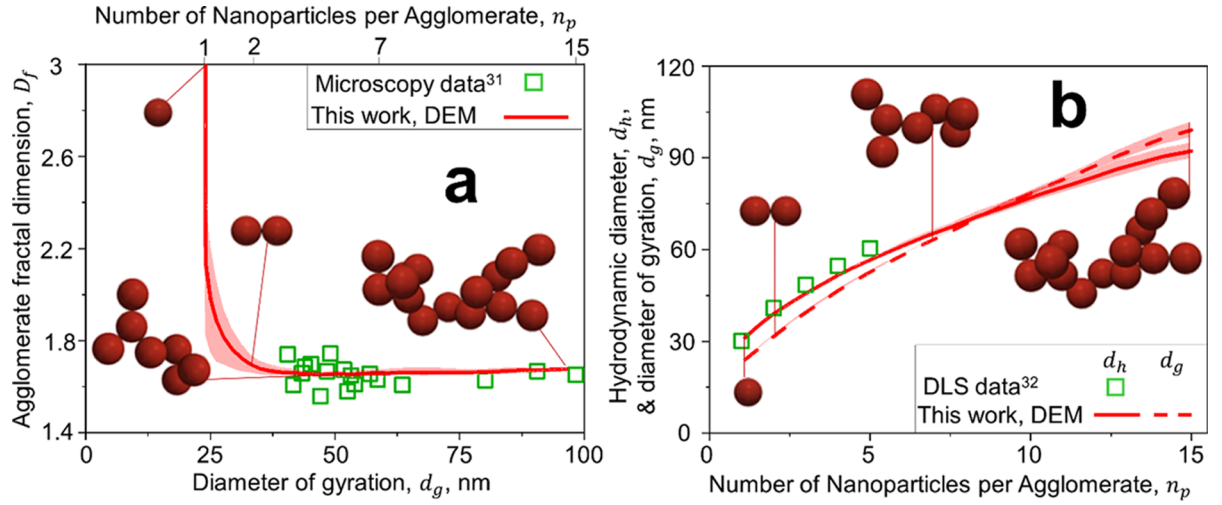

Figure 1. (a) Evolution of D_f during agglomeration of gold NPs as a function of their d_g (bottom abscissa) and n_p (top abscissa) derived here by DEM (line and inset agglomerate images) along with microscopy data[31] (symbols). (b) Evolution of d_h (solid line, symbols) and d_g (broken line) of gold NP agglomerates as a function of their n_p derived by DEM (lines and inset images) and measured using dynamic light scattering[32] (DLS; symbols).

agglomerates show a characteristic broad peak[26] with a λ_1 of 650−700 nm. Khlebtsov *et al.*[27] simulated the light absorption of gold NP chains ($D_f = 1$) having 4−36 NPs at s = 1, 2, 5, 10, and 20 nm. In addition, the light absorption by realistic agglomerates with $D_f = 2$ having 2−200 NPs was investigated for s = 0.05 and 1 nm. These coarse-grid DDA[28] and T-matrix[27] simulations underestimate the measured[29] λ_1 redshift by up to 55%. This is due to the low dipole resolution used in DDA that limits the optimization of the λ_1 of agglomerates based on the s of their constituent gold NPs.

Here, a new plasmon ruler for gold agglomerates having s < 10 nm is derived, for the first time to the best of our knowledge, by determining the light extinction of agglomerates during coagulation with discrete element modeling (DEM) interfaced with DDA.[30] These simulations and the plasmon ruler are compared to microscopy,[4,31] dynamic light scattering,[32] analytical centrifugation,[29] and UV−visible spectroscopy data.[4,5,29,33,34] This set of data is the largest ever for benchmarking plasmon rulers, to the best of our knowledge.

2. METHODS

2.1. DEM of Gold NP Agglomerates. Brownian coagulation or agglomeration of gold NPs in the absence of sintering or coalescence is described by DEM neglecting van der Waals, electric, and hydrodynamic forces.[23] Such DEM-derived coagulation dynamics have been validated in detail for organic (*e.g.*, nascent[35] and mature soot[36]) and inorganic (*e.g.*, zirconia,[37] silica,[38] and gold[39]) agglomerates dispersed in air and water[40] at a wide range of particle concentrations.[41] Here, 1000 monodisperse gold primary particles with a diameter d_p = 20−80 nm (that cover the entire range of gold NPs used in the UV−vis spectroscopy data[4,5,29,33,34] presented in Figures 2, 3, and 5) are randomly distributed in a cubic cell containing water at 1 atm and 300 K, applying periodic boundary conditions.[35] These conditions are commonly used for the wet-phase synthesis of gold NP agglomerates.[29] Therefore, agglomerates consisting of 2−15 monodisperse NPs are formed. The distance s between constituent gold NPs is varied between 1 and 50 nm by adjusting their center of mass to account for organic[29] and inorganic[5] coatings that are used experimentally to optimize the optical properties of gold agglomerates. Quantum tunnelling effects are negligible for the present s range (1−50 nm).[42] The composition of such coatings may enhance λ_1 by 5−9% depending on their refractive index.[1] The n_p, d_h, and d_g of these DEM-derived agglomerates are determined[23,35] accounting for their detailed morphology. In particular, the d_h of NP agglomerates having n_p < 100 is[43]

$$d_h = d_p n_p^{0.46} \tag{1}$$

while their d_g is[44]

$$d_g^2 = 4\frac{\sum_i x_i^2 m_i}{\sum_i m_i} \tag{2}$$

where m_i is the mass, and x_i is the distance of primary particle i to the agglomerate center of mass. The agglomerate d_g is related to d_p and n_p by a power law[45]

$$n_p = k_n\left(\frac{d_g}{d_p}\right)^{D_f} \tag{3}$$

where D_f and k_n are the fractal dimension and prefactor, respectively. The morphology of DEM-derived agglomerates has been validated already with helium ion microscopy,[35] light scattering,[36] and mass-mobility measurements of nascent[35] and mature[36] soot, zirconia,[37] silica,[38] and gold[39] NPs.

2.2. Gold Optical Properties by DDA. DDA is used to estimate light absorption, scattering, and extinction of DEM-derived agglomerates of gold NPs using the open-source DDSCAT 7.3 code.[46] The DEM-derived, fractal-like agglomerate morphology is represented on a lattice by an array of discrete dipoles interacting with each other through their electric fields.[46] The dipole electric properties are described by the input bulk gold refractive index,[47] *RI*, which is valid for the d_p = 20−80 nm investigated here.[48] Maxwell's equations are discretized on the lattice using the volume integral equation method and solved iteratively.[46]

The dipole spacing, x, must be small[46] compared to the incident light wavelength, λ, to calculate accurately the gold

https://doi.org/10.1021/acs.analchem.1c05145
Anal. Chem. 2022, 94, 5310−5316

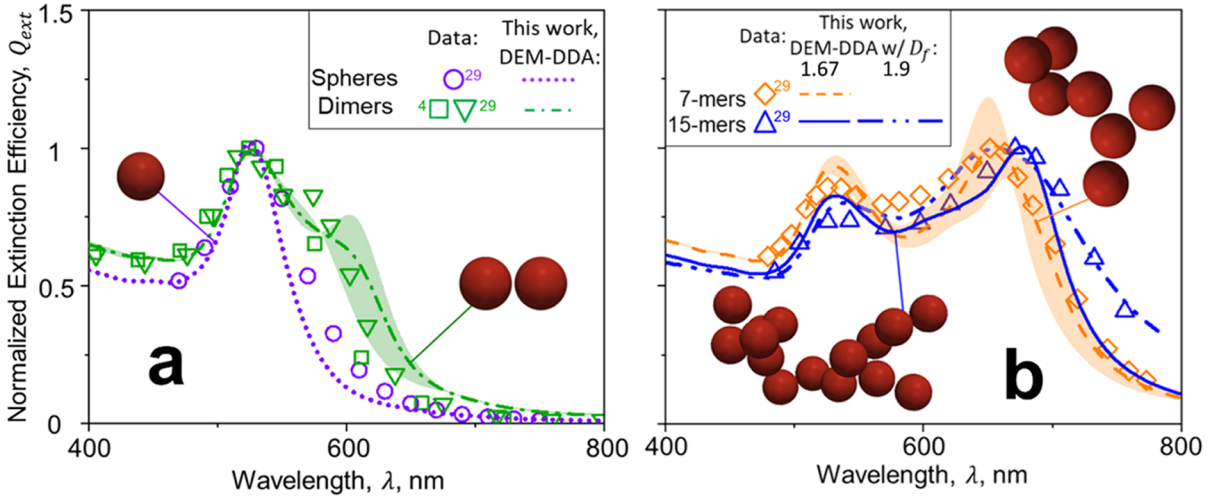

Figure 2. Normalized Q_{ext} as a function of λ of gold (a) spheres (dotted line, circles), dimers (dot-broken line, squares, inverse triangles), (b) 7- (broken line, diamonds) and 15-mers (solid and double dot-broken lines, triangles) with D_f = 1.67 (dot-broken, broken, and solid lines) or 1.9 (double dot-broken lines) estimated here by DDA (lines) and compared to those measured by Zook *et al.*[29] (circles, diamonds, and triangles) and Esashika *et al.*[4] (squares and inverse triangles). The DDA-derived Q_{ext} of gold NPs increases as single spheres (dotted line) form dimers (dot-broken line), 7- (broken line), and 15-mers (solid line) by agglomeration shifting λ_l from 530 to 680 nm, in excellent agreement with data[4,29] (symbols).

extinction coefficient, Q_{ext}, that accounts for both light absorption and scattering of gold NPs. Owing to the high light extinction of gold NPs in the NIR, x is varied for different λ and RI to have a constant ratio of $2\pi|RI|x/\lambda = 0.0192$. This precision criterion is up to 16 times smaller than those used for other strongly absorbing materials (*e.g.*, soot[30]) and results in 100,000 dipoles per gold primary particle.

3. RESULTS AND DISCUSSION

3.1. Validation of Au Agglomerate Morphology and Optical Properties. Agglomerates of gold NPs of diameter d_p = 30 nm with well-defined morphology characteristics were created by DEM. Figure 1a shows the evolution of their D_f (line and insets) during growth by coagulation as a function of their average diameter of gyration, d_g (bottom abscissa), or the number of constituent NPs per agglomerate, n_p (top abscissa). The shaded area indicates the statistical variation of DEM. These D_f dynamics are compared to microscopy data of gold NP agglomerates with similar d_g (symbols)[31] from microscopy images based on the measured bounding length.[49] The DEM-derived D_f evolution shown in Figure 1a was obtained using d_p = 30 nm to be consistent with the d_p range that is relevant for UV−vis spectroscopy measurements.[4,5,29,33,34] The D_f was measured by Grogan *et al.*[31] for NPs with d_p = 5 nm. Decreasing d_p from 30 to 5 nm increases D_f by 3−9% (as shown in Figure 5a of ref 23). This is on par with the statistical variation of the DEM simulations (shaded area) and experiments[31] shown in Figure 1a.

As single spherical Au NPs coagulate and form agglomerates, their D_f decreases from 3 to about 1.6−1.7 for d_g > 40 nm or n_p > 3. The D_f is slightly smaller than the classic limit of D_f = 1.78 ± 0.05 obtained by diffusion-limited cluster agglomeration[50] as their n_p is rather small (n_p < 20) for this asymptotic D_f.[23] Nevertheless, the evolution of D_f (Figure 1a, line) is in excellent agreement with microscopy data[31] of gold agglomerates of similarly small n_p (Figure 1a, symbols) pointing out the validity of DEM.

Figure 1b shows the hydrodynamic diameter, d_h (solid line, symbols), and d_g (broken line) of Au agglomerates as a function of n_p derived by DEM (lines) and measured using dynamic light scattering[32] (DLS; symbols). The d_h and d_g are the diameters of drag- and inertia-equivalent spheres, respectively.[51] For example, single spheres of d_h = 30 nm have $d_g = d_h/1.29$.[51] During coagulation, d_h and d_g increase with increasing n_p based on eqs 1 and 3, respectively (see Methods). This results in 7- and 15-mers having $d_h = d_g$ and $d_h = 0.9d_g$, respectively. The latter is consistent with Stokesian dynamics of agglomerates[52] having similar n_p. The d_h of all agglomerates is smaller than 120 nm, the desirable d_h range for drug delivery.[53] The good agreement of DEM-derived D_f and d_h with microscopy (Figure 1a) and light scattering measurements (Figure 1b), respectively, further validates the present simulations.

Next, these realistic agglomerates were used for determining their light extinction by DDA. Figure 2 shows the normalized extinction spectra of gold (a) spheres (dotted line, circles[29]) and dimers (dot-broken line, squares,[4] inverse triangles[29]), as well as of (b) the above 7- (broken line, diamonds[29]) and 15-mers (solid & double dot-broken lines, triangles[29]) with D_f = 1.67 (dot-broken, broken and solid lines) or 1.9 (double dot-broken lines). The D_f = 1.9 is selected as an average between the D_f = 1.78 and 2 of agglomerates obtained by coagulation[23] and break up in the presence of van der Waals, hydrodynamic (*e.g.*, shear)[24] or electric forces,[25] respectively, at long residence times during drug delivery. Lines correspond to present simulations and symbols to data by Zook *et al.*[29] (circles, diamonds, and triangles) and Esashika *et al.*[4] (squares and inverse triangles). All extinction spectra were obtained from Au agglomerates with the NP d_p = 20−30 nm and s = 1.4 nm. The shaded areas indicate the DDA variation between d_p = 20 and 30 nm for four dimers (Figure 2a) and 7-mers (Figure 2b). The measured and simulated light extinction spectra are normalized with the maximum extinction efficiency, Q_{ext}.

The DDA-derived Q_{ext} of single gold NPs with d_p = 30 nm (Figure 2a) attains its maximum at a transverse λ_s of about 530 nm (dotted line), consistent with measurements[29] (circles).

https://doi.org/10.1021/acs.analchem.1c05145
Anal. Chem. 2022, 94, 5310−5316

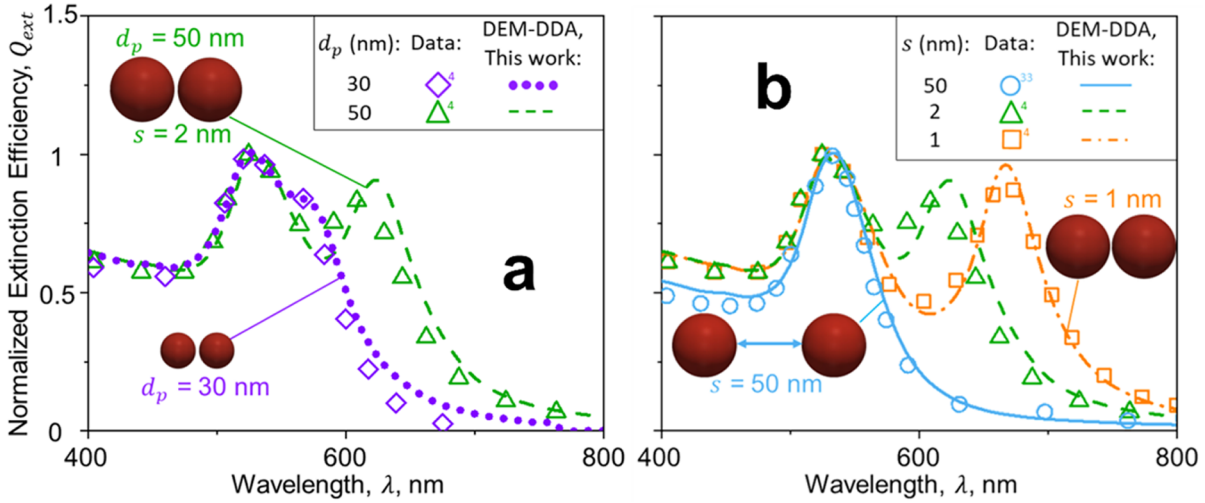

Figure 3. Normalized Q_{ext} as a function of λ of gold dimers with d_p = 30 (a: dotted line) or 50 nm (b) at s = 50 (solid line), 2 (broken & dotted lines, triangles, and diamonds), and 1 nm (dot-broken line, squares) estimated here by DDA (lines) and measured using UV−visible spectroscopy and microscopy[4,33] (symbols).

The light extinction spectrum obtained by DDA for dimers of such gold NPs also exhibits a minor peak at λ_l = 600 nm due to plasmonic coupling.[1] This peak becomes more significant with 7- and 15-mers (Figure 2b, broken and solid lines), shifting λ_l up to 680 nm. The λ_l increases only by 10% as 7-mers grow into 15-mers, in good agreement with the data.[29] The small sensitivity of λ_l on the gold agglomerate n_p suggests that the light extinction derived here by DEM-DDA for n_p = 7 and 15 is also valid for larger agglomerates consistent with Khlebtsov *et al.*[27] and may not depend strongly on individual agglomerate n_p and D_f. However, previous simulations using a single dipole per NP showed that the λ_l of gold agglomerates increases only up to 600 nm.[28] Here, the maximum λ_l = 680 nm obtained from 15-mers using 100′000 dipoles per NP (lines) is in excellent agreement with the measured λ_l range of 650−700 nm[23] (Figure 2b, triangles). Increasing D_f from 1.67 to 1.9 broadens the light extinction spectra of 15-mers (again in agreement with data) but hardly affects their λ_l (double dot-broken line). Therefore, the plasmon ruler derived here based on λ_l is not affected by van der Waals, hydrodynamic, and electric forces.

The electric field enhancement by plasmonic coupling depends on d_p and s, affecting the light extinction of Au agglomerates.[54] Figure 3a shows the normalized extinction spectra of gold dimers with d_p = 30 (dotted line, diamonds[4]) and 50 nm (broken line, triangles[4]) at s = 2 nm derived here by DDA (lines) and compared to UV−visible spectroscopy and microscopy measurements (symbols[4]). Increasing d_p from 30 to 50 nm enhances the plasmonic coupling between gold NPs and increases their λ_l from 580 to 620 nm, in good agreement with the data[4] (symbols).

Similarly, Figure 3b shows the normalized extinction spectra of gold dimers (d_p = 50 nm) at s = 50 (solid line, circles[33]), 2 (broken line, triangles[4]), and 1 nm (dot-broken line, squares[4]) estimated here by DDA (lines) along with UV−visible spectroscopy and microscopy[4,33] measurements (symbols). The Q_{ext} of dimers of spheres with d_p = 50 nm each at s = 50 nm that practically corresponds to single ones is in excellent agreement with that measured by UV−visible spectroscopy from single spheres[33] for all λ. As the s of these dimers decreases to 2 and 1 nm, the Q_{ext} exhibits a second maximum at the longitudinal λ_l from the electric field enhancement induced by plasmonic coupling.[55] The λ_l redshifts with decreasing s, consistent with previous DDA simulations[3] and is in excellent agreement with data[4] (symbols). This redshift of λ_l increases the light extinction of gold dimers in the NIR, consistent with the light absorption measurements of Au NPs separated by silica coatings of various thicknesses,[5] further validating the present DEM-DDA methodology.

3.2. Plasmon Ruler for Au Nanoagglomerates. Figure 4 shows the λ_l as a function of s/d_p by DEM-DDA for dimers of monodisperse (squares and inverse triangles) and bidisperse (circles) NPs, and DEM-derived 7- (diamonds) and 15-mers (triangles) of monodisperse NPs with d_p = 20−50 nm (squares, circles, diamonds, triangles) or 75 and 80 nm (inverse triangles) and s = 1−50 nm. Dimers with d_p = 75−80

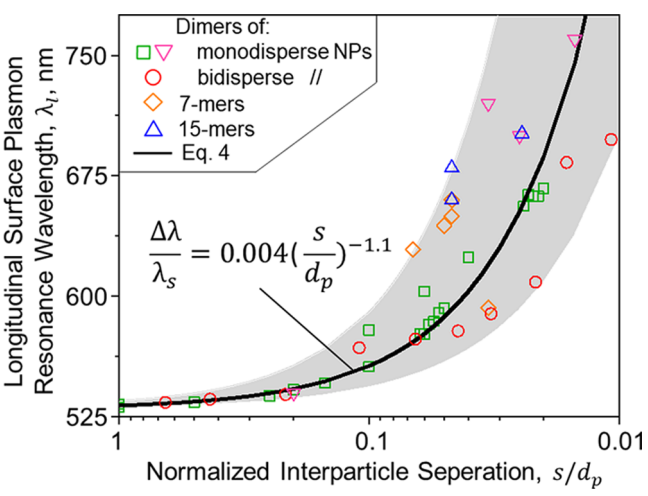

Figure 4. Au agglomerate λ_l as a function of normalized interparticle separation, s/d_p, estimated by DDA using dimers of monodisperse (squares and inverse triangles) and bidisperse (circles) NPs, and DEM-derived 7- (diamonds) and 15-mers (triangles) of monodisperse NPs with d_p = 20−50 (squares, circles, diamonds, and triangles) or 75 and 80 nm (inverse triangles) and s = 1−50 nm. A new plasmon ruler (eq 4, solid line and shaded area) is derived by regressing the DDA-derived λ_l evolution.

https://doi.org/10.1021/acs.analchem.1c05145
Anal. Chem. 2022, 94, 5310−5316

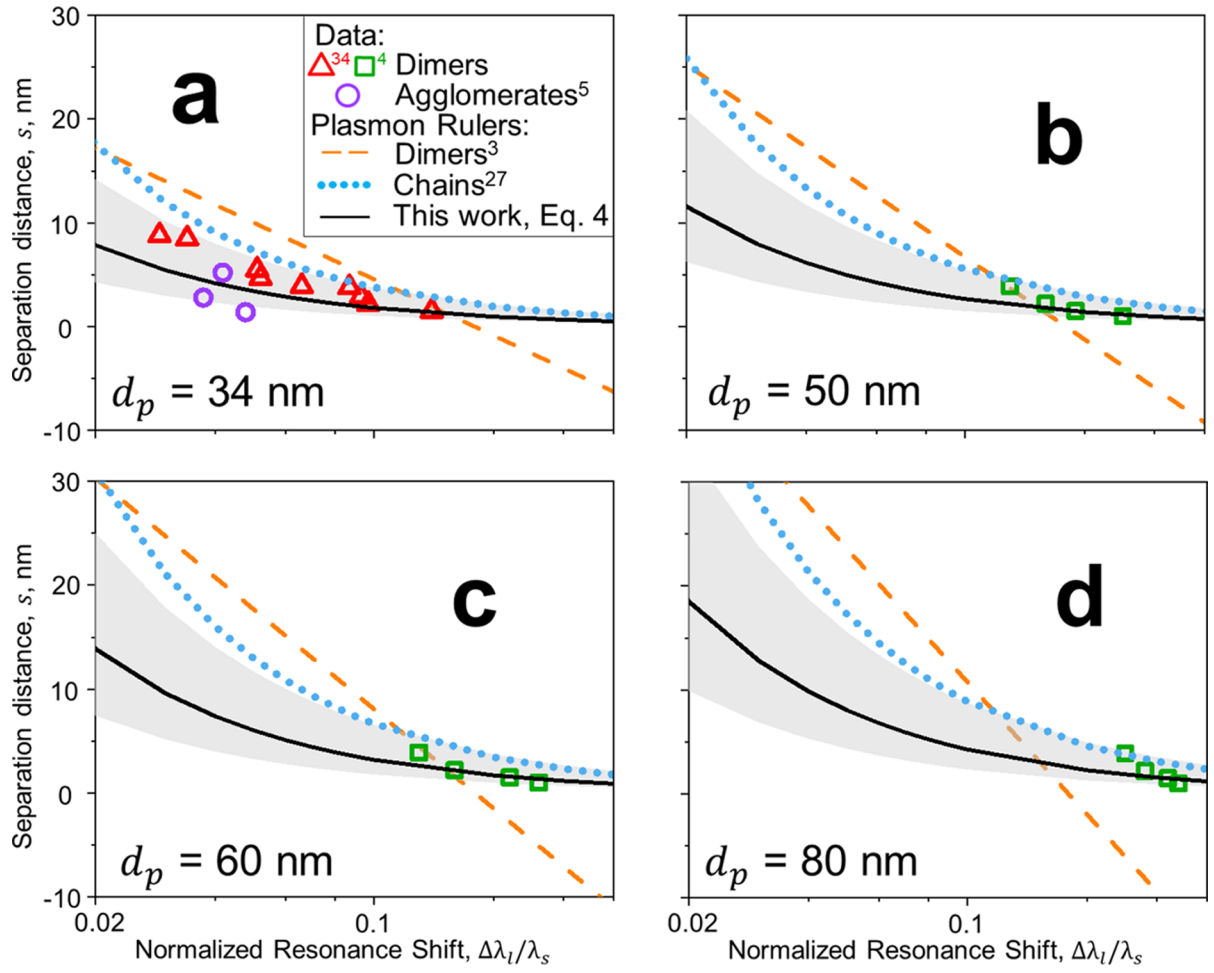

Figure 5. Estimated interparticle separation distance, s, as a function of normalized λ_l shift, $\Delta\lambda/\lambda_s$, using plasmon rulers for chains[27] (dotted line), dimers[3] (broken line), and 7- and 15-mers (eq 4, solid line) of gold NPs with d_p = 34 (a), 50 (b), 60 (c), and 80 nm (d) compared to microscopy and UV−visible measurements of dimers (triangles,[34] and squares[4]) and agglomerates (circles[5]).

nm have 7% larger λ_l than those with d_p = 20−50 nm at s/d_p = 0.025. Similarly, increasing the NP polydispersity decreases the λ_l of dimers by about 8% at s/d_p = 0.02−0.04. The above small reductions are within the statistical variability of the DEM-DDA simulations (shaded area). By regressing s/d_p to the ratio of $\Delta\lambda = \lambda_l - \lambda_s$ to λ_s = 530 nm corresponding to a Au sphere suspended in water,[3] a new plasmon ruler is created (Figure 4, solid line):

$$\frac{\Delta\lambda}{\lambda_s} = 0.004\left(\frac{s}{d_p}\right)^{-1.1} \quad (4)$$

Equation 4 has been derived for gold NPs with d_p < 100 nm and is not affected by dynamic depolarization and structural retardation.[56] The light extinction of such NPs is given only by their dipole mode resulting in $\lambda_s \sim$ 530 nm.[27] Therefore, the critical diameter for this ruler is 100 nm, as the light extinction of gold NPs with d_p > 100 nm is determined by the sum of both the dipole and quadrupole modes and increases their λ_s > 530 nm.[27] Furthermore, eq 4 is valid for agglomerates with $s \geq$ 1 nm that are not affected by quantum tunneling[6] and the quenched near-field intensity.[7]

Next, eq 4 is compared to the experimental data and previously reported plasmon rulers. Figure 5 shows the estimated s (lines) as a function of the normalized λ_l shift, $\Delta\lambda/\lambda_s$, using plasmon rulers for chains (dotted line),[27] dimers (broken line),[3] and 7- and 15-mers (eq 4, solid line) of gold NPs with d_p = 34 (a), 50 (b), 60 (c), and 80 nm (d) in comparison to microscopy and UV−vis measurements of dimers (triangles,[34] and squares[4]) and agglomerates (circles[5]). Jain *et al.*[3] derived and validated their plasmon ruler for dimers at s > 10 nm. Below 10 nm, this ruler (broken line) results in an error of 220% on average. The plasmon ruler of Khlebtsov *et al.*[27] was derived for chains with D_f = 1 at s = 1−20 nm (dotted line) and is in better agreement with data. Nevertheless, it still overestimates the measured s by 70% (on average) due to the neglect of the realistic structure of agglomerates (D_f > 1) that are commonly present in measurements. In contrast, the plasmon ruler derived here with D_f = 1.67−1.9 (solid line and within its shade) is in better agreement with the data for all d_p studied here.

Therefore, eq 4 can be used to measure and accurately select sub-10 nm organic and inorganic coatings of gold nanoagglomerates and to monitor the dynamics of biomolecules. For example, during protein adsorption on the NP surface, a corona monolayer is formed.[57] The monolayer thickness may vary from 3.3[58] to 16 nm[59] depending on the adsorbed protein[57] and its concentration,[60] as well as the NP size[59] and surface charge.[61] The protein corona monolayer is formed within 10−50 min and covers up to 80% of the particle

https://doi.org/10.1021/acs.analchem.1c05145
Anal. Chem. 2022, 94, 5310−5316

surface.[60] At such long residence times, gold NPs coagulate into agglomerates with various s.[11] In specific, Figure 6 shows

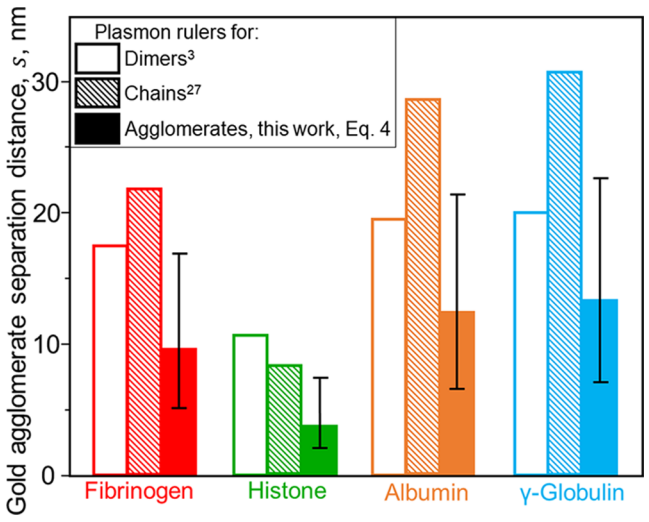

Figure 6. Separation distance, s, of gold agglomerates with d_p = 30 nm coated by fibrinogen (red), histone (green), albumin (orange), and γ-globulin (blue) estimated using UV−vis spectroscopy data[11] with plasmon rulers for dimers[3] (open bars), chains[27] (lines bars) and agglomerates (eq 4, filled bars).

the s of gold agglomerates with d_p = 30 nm coated by common blood proteins, that is, fibrinogen (red), histone (green), albumin (orange), and γ-globulin (blue) estimated by interfacing UV−vis spectroscopy data[11] with eq 4 (filled bars). The gold agglomerate s ranges from 3.9 (histone, green filled bar) to 13.3 nm (blue filled bar). In this regard, using plasmon rulers for gold dimers[3] (open bars) and chains[27] (lined bars) overestimates by up to a factor of 2.8 and 2.3 , the gold agglomerate s formed by histone (green filled bar) and γ-globulin (blue filled bar), respectively. Therefore, the sub-10 nm ruler derived here for gold NP agglomerates is essential to accurately monitor the dynamics of protein corona formation.

4. SUMMARY & CONCLUSIONS

The evolution of gold agglomerate morphology and optical properties during agglomeration is investigated here by coupling DEM with DDA. The morphology and hydrodynamic diameter of DEM-derived gold NP agglomerates are validated with microscopy[31] and light scattering[32] measurements, respectively. The evolution of gold light extinction during agglomeration reveals that the longitudinal surface plasmon resonance wavelength, λ_l, increases up to 680 nm as single gold NPs coagulate to 15-mers, in excellent agreement with data from UV−visible spectroscopy.[4,29]

The λ_l shift of gold dimers, 7-, and 15-mers increases with decreasing s and can be described by a universal power law resulting in a new plasmon ruler (eq 4) that enables the estimation of Au nanoagglomerate coating thickness, s, in excellent agreement with the microscopy data.[4,5,34] In contrast, existing, widely used plasmon rulers for dimers[3] and chains[27] estimate coating thicknesses smaller than 10 nm with an average error of 220 and 70%, respectively. Therefore, the new plasmon ruler obtained here for agglomerates of Au NPs can be used instead of tedious microscopy measurements to determine the thickness of sub-10 nm organic and inorganic coatings. This can facilitate monitoring of the dynamics of biomolecules, such as proteins[10] and DNA,[12] and the optimization of gold agglomerate coating thickness for photothermal therapy of cancer.[5]

AUTHOR INFORMATION

Corresponding Author

Sotiris E. Pratsinis − *Particle Technology Laboratory, Department of Mechanical and Process Engineering, Institute of Energy & Process Engineering, ETH Zürich, Zürich CH-8092, Switzerland*; Phone: +41 (0) 44 632 31 8110; Email: sotiris.pratsinis@ptl.mavt.ethz.ch; Fax: +41 (0) 44 632 15 95

Authors

Georgios A. Kelesidis − *Particle Technology Laboratory, Department of Mechanical and Process Engineering, Institute of Energy & Process Engineering, ETH Zürich, Zürich CH-8092, Switzerland*; orcid.org/0000-0003-4220-9649

Daniel Gao − *Particle Technology Laboratory, Department of Mechanical and Process Engineering, Institute of Energy & Process Engineering, ETH Zürich, Zürich CH-8092, Switzerland*

Fabian H.L. Starsich − *Nanoparticle Systems Engineering Laboratory, Department of Mechanical and Process Engineering, Institute of Energy & Process Engineering, ETH Zürich, Zürich CH-8092, Switzerland; Particles-Biology Interactions, Department Materials Meet Life, Swiss Federal Laboratories for Materials Science and Technology (Empa), St. Gallen CH-9014, Switzerland*

Complete contact information is available at: https://pubs.acs.org/10.1021/acs.analchem.1c05145

Notes

The authors declare no competing financial interest.

ACKNOWLEDGMENTS

This research was funded by the Swiss National Science Foundation (206021_183298, 200020_182668, 250320_163243, and 206021_170729) and the ETH Zurich and Stavros Niarchos Foundations (ETH-08 14-2). An early version of this research received the Best Poster Award at the symposium on "Emerging Material Platforms and Approaches for Plasmonics, Metamaterials, and Metasurfaces" of the 2019 Fall Meeting of the Material Research Society (Dec. 1−6, 2019, Boston, MA, USA). The authors gratefully acknowledge help from S. Benz and G.P. Rivano with the DDA simulations.

REFERENCES

(1) Jain, P. K.; El-Sayed, M. A. *Chem. Phys. Lett.* **2010**, *487*, 153−164.

(2) Halas, N. J.; Lal, S.; Chang, W.-S.; Link, S.; Nordlander, P. *Chem. Rev.* **2011**, *111*, 3913−3961.

(3) Jain, P. K.; Huang, W.; El-Sayed, M. A. *Nano Lett.* **2007**, *7*, 2080−2088.

(4) Esashika, K.; Ishii, R.; Tokihiro, S.; Saiki, T. *Opt. Mater. Express* **2019**, *9*, 1667−1677.

(5) Sotiriou, G. A.; Starsich, F.; Dasargyri, A.; Wurnig, M. C.; Krumeich, F.; Boss, A.; Leroux, J.-C.; Pratsinis, S. E. *Adv. Funct. Mater.* **2014**, *24*, 2818−2827.

(6) Zuloaga, J.; Prodan, E.; Nordlander, P. *Nano Lett.* **2009**, *9*, 887−891.

(7) García de Abajo, F. J. *J. Phys. Chem. C* **2008**, *112*, 17983−17987.

(8) Fernandez-Leiro, R.; Scheres, S. H. W. *Nature* **2016**, *537*, 339−346.

(9) Weiss, S. *Science* **1999**, *283*, 1676−1683.
(10) Aćimović, S. S.; Kreuzer, M. P.; González, M. U.; Quidant, R. *ACS Nano* **2009**, *3*, 1231−1237.
(11) Lacerda, S. H. D. P.; Park, J. J.; Meuse, C.; Pristinski, D.; Becker, M. L.; Karim, A.; Douglas, J. F. *ACS Nano* **2010**, *4*, 365−379.
(12) Lee, S. E.; Chen, Q.; Bhat, R.; Petkiewicz, S.; Smith, J. M.; Ferry, V. E.; Correia, A. L.; Alivisatos, A. P.; Bissell, M. J. *Nano Lett.* **2015**, *15*, 4564−4570.
(13) Ye, W.; Götz, M.; Celiksoy, S.; Tüting, L.; Ratzke, C.; Prasad, J.; Ricken, J.; Wegner, S. V.; Ahijado-Guzmán, R.; Hugel, T.; Sönnichsen, C. *Nano Lett.* **2018**, *18*, 6633−6637.
(14) Visser, E. W. A.; Horáček, M.; Zijlstra, P. *Nano Lett.* **2018**, *18*, 7927−7934.
(15) Reinhard, B. M.; Siu, M.; Agarwal, H.; Alivisatos, A. P.; Liphardt, J. *Nano Lett.* **2005**, *5*, 2246−2252.
(16) Singh, A. K.; Khan, S. A.; Fan, Z.; Demeritte, T.; Senapati, D.; Kanchanapally, R.; Ray, P. C. *J. Am. Chem. Soc.* **2012**, *134*, 8662−8669.
(17) Hill, R. T.; Mock, J. J.; Hucknall, A.; Wolter, S. D.; Jokerst, N. M.; Smith, D. R.; Chilkoti, A. *ACS Nano* **2012**, *6*, 9237−9246.
(18) Readman, C.; de Nijs, B.; Szabó, I.; Demetriadou, A.; Greenhalgh, R.; Durkan, C.; Rosta, E.; Scherman, O. A.; Baumberg, J. J. *Nano Lett.* **2019**, *19*, 2051−2058.
(19) Xu, L.; Sun, M.; Ma, W.; Kuang, H.; Xu, C. *Mater. Today* **2016**, *19*, 595−606.
(20) Valencia, P. M.; Farokhzad, O. C.; Karnik, R.; Langer, R. *Nat. Nanotechnol.* **2012**, *7*, 623−629.
(21) Starsich, F. H. L.; Herrmann, I. K.; Pratsinis, S. E. *Annu. Rev. Chem. Biomol. Eng.* **2019**, *10*, 155−174.
(22) Sun, M.; Xu, L.; Bahng, J. H.; Kuang, H.; Alben, S.; Kotov, N. A.; Xu, C. *Nat. Commun.* **2017**, *8*, 1847−1851.
(23) Goudeli, E.; Eggersdorfer, M. L.; Pratsinis, S. E. *Langmuir* **2015**, *31*, 1320−1327.
(24) Eggersdorfer, M. L.; Kadau, D.; Herrmann, H. J.; Pratsinis, S. E. *J. Colloid Interface Sci.* **2010**, *342*, 261−268.
(25) Peng, Z.; Doroodchi, E.; Evans, G. *Powder Technol.* **2010**, *204*, 91−102.
(26) Doyen, M.; Goole, J.; Bartik, K.; Bruylants, G. *J. Colloid Interface Sci.* **2016**, *464*, 160−166.
(27) Khlebtsov, B.; Zharov, V.; Melnikov, A.; Tuchin, V.; Khlebtsov, N. *Nanotechnology* **2006**, *17*, 5167−5179.
(28) Khlebtsov, N. G.; Dykman, L. A.; Krasnov, Y. M.; Mel'nikov, A. G. *Colloid J.* **2000**, *62*, 765−779.
(29) Zook, J. M.; Rastogi, V.; MacCuspie, R. I.; Keene, A. M.; Fagan, J. *ACS Nano* **2011**, *5*, 8070−8079.
(30) Kelesidis, G. A.; Pratsinis, S. E. *Proc. Combust. Inst.* **2019**, *37*, 1177−1184.
(31) Grogan, J. M.; Rotkina, L.; Bau, H. H. *Phys. Rev. E: Stat., Nonlinear, Soft Matter Phys.* **2011**, *83*, 061405.
(32) Tsai, D.-H.; Cho, T. J.; DelRio, F. W.; Taurozzi, J.; Zachariah, M. R.; Hackley, V. A. *J. Am. Chem. Soc.* **2011**, *133*, 8884−8887.
(33) Martinsson, E.; Sepulveda, B.; Chen, P.; Elfwing, A.; Liedberg, B.; Aili, D. *Plasmonics* **2014**, *9*, 773−780.
(34) Kadkhodazadeh, S.; de Lasson, J. R.; Beleggia, M.; Kneipp, H.; Wagner, J. B.; Kneipp, K. *J. Phys. Chem. C* **2014**, *118*, 5478−5485.
(35) Kelesidis, G. A.; Goudeli, E.; Pratsinis, S. E. *Proc. Combust. Inst.* **2017**, *36*, 29−50.
(36) Kelesidis, G. A.; Goudeli, E.; Pratsinis, S. E. *Carbon* **2017**, *121*, 527−535.
(37) Goudeli, E.; Gröhn, A. J.; Pratsinis, S. E. *Aerosol Sci. Technol.* **2016**, *50*, 591−604.
(38) Kelesidis, G. A.; Furrer, F. M.; Wegner, K.; Pratsinis, S. E. *Langmuir* **2018**, *34*, 8532−8541.
(39) Kelesidis, G. A.; Pratsinis, S. E. *Chem. Eng. J.* **2021**, *421*, 129884.
(40) Spyrogianni, A.; Karadima, K. S.; Goudeli, E.; Mavrantzas, V. G.; Pratsinis, S. E. *J. Chem. Phys.* **2018**, *148*, 064703.
(41) Heine, M. C.; Pratsinis, S. E. *Langmuir* **2007**, *23*, 9882−9890.
(42) Zhu, W.; Esteban, R.; Borisov, A. G.; Baumberg, J. J.; Nordlander, P.; Lezec, H. J.; Aizpurua, J.; Crozier, K. B. *Nat. Commun.* **2016**, *7*, 11495−11501.
(43) Sorensen, C. M. *Aerosol Sci. Technol.* **2011**, *45*, 765−779.
(44) Eggersdorfer, M. L.; Pratsinis, S. E. *Aerosol Sci. Technol.* **2012**, *46*, 347−353.
(45) Medalia, A. I. *J. Colloid Interface Sci.* **1967**, *24*, 393−404.
(46) Draine, B. T.; Flatau, P. J. *J. Opt. Soc. Am. A* **1994**, *11*, 1491−1499.
(47) Johnson, P. B.; Christy, R. W. *Phys. Rev. B* **1972**, *6*, 4370−4379.
(48) Qin, J.; Peng, Z.; Li, B.; Ye, K.; Zhang, Y.; Yuan, F.; Yang, X.; Huang, L.; Hu, J.; Lu, X. *Nanoscale* **2015**, *7*, 13991−14001.
(49) Brasil, A. M.; Farias, T. L.; Carvalho, M. G. *J. Aerosol Sci.* **1999**, *30*, 1379−1389.
(50) Jullien, R.; Kolb, M.; Botet, R. *J. Phys.* **1984**, *45*, 395−399.
(51) Eggersdorfer, M. L.; Pratsinis, S. E. *Adv. Powder Technol.* **2014**, *25*, 71−90.
(52) Filippov, A. V. *J. Colloid Interface Sci.* **2000**, *229*, 184−195.
(53) Blanco, E.; Shen, H.; Ferrari, M. *Nat. Biotechnol.* **2015**, *33*, 941−951.
(54) Hao, E.; Schatz, G. C. *J. Chem. Phys.* **2004**, *120*, 357−366.
(55) Willets, K. A.; Van Duyne, R. P. *Annu. Rev. Phys. Chem.* **2007**, *58*, 267−297.
(56) Ben, X.; Park, H. S. *J. Phys. Chem. C* **2011**, *115*, 15915−15926 and erratum: ibid 2012, 116, 8857, doi.org/10.1021/jp3025254.
(57) Shang, L.; Nienhaus, G. U. *Acc. Chem. Res.* **2017**, *50*, 387−395.
(58) Maffre, P.; Nienhaus, K.; Amin, F.; Parak, W. J.; Nienhaus, G. U. *Beilstein J. Nanotechnol.* **2011**, *2*, 374−383.
(59) Piella, J.; Bastús, N. G.; Puntes, V. *Bioconjugate Chem.* **2017**, *28*, 88−97.
(60) Vilanova, O.; Mittag, J. J.; Kelly, P. M.; Milani, S.; Dawson, K. A.; Rädler, J. O.; Franzese, G. *ACS Nano* **2016**, *10*, 10842−10850.
(61) Treuel, L.; Brandholt, S.; Maffre, P.; Wiegele, S.; Shang, L.; Nienhaus, G. U. *ACS Nano* **2014**, *8*, 503−513.

https://doi.org/10.1021/acs.analchem.1c05145
Anal. Chem. 2022, 94, 5310−5316